# **Fast Dynamics of Brain-wide Patterns on Neuronal Oscillations**

Lei Ding<sup>1,2</sup>, Member, IEEE, Han Yuan<sup>1,2</sup>, Member, IEEE

<sup>1</sup>Stephenson School of Biomedical Engineering, <sup>2</sup>Institute for Biomedical Engineering, Science and Technology, University of Oklahoma, Norman, OK 73072 USA

#### **ABSTRACT**

Various neuroimaging techniques and data analytics have been established in studying brain-wide activations in human. However, a significant impediment in studying brain-wide activations have been limited in its temporal resolutions, due to either slow response times in the signal of interest or amount of data required by the special analytics used. To overcome these limitations, we have developed modeling and computational tools for noninvasive electrical imaging of fast brain-wide neuronal activations in human brains from highdensity electroencephalography (EEG). Here we report a set of brain-wide co-activation patterns (bwCAPs) at the timescales of tens of milliseconds from dominant resting rhythmic human EEG at the alpha band, which indicate multiple recurring transient brain states and a well-organized transitional structure among them. This is the first time in detecting brain-wide modulating patterns on the wellestablished neuronal oscillation. Due to the distributed nature of these bwCAPs at the brain-wide scale, their timescales close to the actual neuronal events, and frequency-specific detections, we expect that these phenomena will support future investigations on human cognition noninvasively.

*Index Terms*— EEG, CAP, brain-wide, neuronal oscillation, fast dynamics

#### 1. INTRODUCTION

Versatility of human cognition relies on the global access to widely distributed information across the entire brain at rapid speeds. The hierarchical network constructs of human brains at multiple spatial scales provide such a global access. At the macroscopic level, data from recent functional neuroimaging studies have provided strong evidence on mechanistic roles of brain-wide networks in cognition/behaviors [1, 2]. Specifically, these brain-wide networks/patterns have been widely elucidated in functional magnetic resonance imaging (fMRI) [3, 4], via measuring time-domain functional connectivity (FC) in either resting-state/task-free period [4], i.e., resting state networks (RSN), or tasks [5]. As fMRI is limited by the "sluggish" nature of hemodynamic responses of several seconds [6], studies using electroencephalography (EEG) [7, 8] and magnetoencephalography (MEG) [9] have reported brain-wide networks, e.g., RSNs in particular. These EEG/MEG RSNs have shown spatial similarities to fMRI

RSNs [9] and strong temporal correspondences have been demonstrated in RSNs from simultaneously recorded EEG and fMRI data [7]. However, brain-wide networks reported in EEG/MEG are still limited in temporal resolutions due to the use of similar time-domain FC measures as in fMRI.

In a long history, fMRI FCs have been measured typically on recorded data of a few minutes using pairwise statistical metrics, e.g., correlation-based analysis (CBA) [10], or data-driven methods, e.g., independent component analysis (ICA) [11, 12]. Both CBA and ICA are time-domain measures, and the temporal resolution of outcomes from such analyses are further dependent on the size of pre-selected time windows beyond the slow hemodynamic responses in fMRI. In recent EEG/MEG studies, these time-domain FC measures have been similarly adopted, both on sensor-level EEG [13-15] and cortical source data reconstructed from EEG/MEG [7, 16, 17] via solving the so-called inverse problem [18-20]. Therefore, while EEG/MEG unsurpassed temporal resolution in recordings, i.e., milliseconds, brain-wide networks estimated EEG/MEG via using time-domain FC measures are limited towards tens of seconds or event minutes.

On the other hand, while brain-wide activations of fast dynamics could not be widely visualized, their existences have been evidenced in frequency-specific neuronal coherence across remote regions within human brains [21]. More recently, via measuring co-fluctuations in time courses of multiple ICs estimated from broadband EEG data, we, for the first time, demonstrated brain-wide co-activation patterns (bwCAPs) of fast dynamics at resting human brains [22]. We have further reported age-dependent changes in temporal and dynamic characteristics of these bwCAPs [23]. However, the physiological mechanism of these bwCAPs has not been elucidated and, especially, it is not clear whether similar bwCAPs exist in band-limited EEG signals that might indicates a potential link to frequency-specific neuronal coherence. In the present study, we extended the measure for co-fluctuations of multiple time courses into a spatial-domain similarity measure in replacing time-domain measures for obtaining brain-wide patterns. We integrated the use of a spatial-domain measure with cortical source tomography estimated from alpha-band EEG signals, which is the dominant rhythmic neural oscillation in resting brains. Our results indicated that transient bwCAPs exist in alpha-band EEG signals and are reproducible at multiple spatial resolutions (i.e., cortical parcels) with similar temporal patterns. Our results further reveal transitional structures among the set of brain states, coded in identified multiple bwCAPs, which might suggest brain-wide neuronal propagations as the mechanism of long-range frequency-specific neuronal coherence.

#### 2. MATERIALS AND METHODS

# 2.1. Data Acquisition and Preprocessing

EEG data used in the present study comprised resting-state recordings from 34 healthy participants (age: 24 ± 5 years, range:18 ~ 38 years, 9 females). Resting-state EEG with eyeclosed were recorded for 10 minutes at a sample frequency of 1000Hz using the 128-channel Amps 300 amplifier (Electrical Geodesics Inc., OR, USA). Structural MRI was acquired via a GE MR750 scanner at the University of Oklahoma Health Science Center (OUHSC) MRI facility, using GE's "BRAVO" sequence: FOV=240 mm, axial slices per slab = 180, slice thickness = 1 mm, image matrix = 256×256, TR/TE = 8.45/3.24 ms. EEG electrode positions and three landmark fiducial locations (i.e., nasion, left and right pre-auricular points) were digitized by the Polhemus Patriot system. Study procedures were approved by the local Institutional Review Board at OUHSC.

EEG data were preprocessed with the same routine at individual participants as reported in our previous study [22] using the EEGLAB toolbox [24]. Briefly, a band-pass filter of 0.5 to 100 Hz and a notch filter of 58 to 62 Hz were firstly applied. Secondly, both automated procedures from the *FASTER* plugin [25] and visual inspection were used to identify noisy channels and artifact independent components (ICs) generated by ocular, muscular and cardiac activities. Identified noisy channels were then interpolated and artifact ICs were removed. At last, EEG data were downsampled to 250 Hz and re-referenced to the common average. It is noted that no bad segments were rejected to maintain the continuity of data for the purpose of calculating temporal and transitional characteristics of bw-CAPs (see section 2.3).

#### 2.2. Cortical Source Tomography

Cortical source tomography was reconstructed distributions of brain sources over the cortical surface from surface EEG recordings. Firstly, to reconstruct cortical sources from EEG, individual MRI was used to build cortical current density (CCD) source models and a three-layer boundary element (BE) volume conductor model using FreeSurfer [26]. The CCD model consisted of 40960 triangular mesh elements and 20484 nodes, while each layer of the volume conduction model consisted of 10242 nodes and 20484 triangles. The nodes on the medial wall adjoining the corpus callosum, basal forebrain, and hippocampus in the CCD model were excluded from the source space for inverse calculation, leading the total number of sources as 18715. The three BE layers corresponded to the scalp, skull, and brain and their electrical conductivities were assigned as  $0.33/\Omega m$ ,  $0.0165/\Omega m$ , and

 $0.33/\Omega m$ , respectively. The registration of EEG electrode locations and the BE model was achieved via aligning three landmark fiducial points from both EEG and MRI. The BE method [27] was used to build the forward relationship between EEG  $\Phi(t)$  and cortical distributed dipole source amplitudes  $\mathbf{S}(t)$ :  $\Phi(t) = \mathbf{L} \cdot \mathbf{S}(t)$ , where  $\mathbf{L}$  is the lead field matrix. The minimum-norm estimate [28] was used to reconstruct dipole source amplitudes:  $\mathbf{S}(t) = \mathbf{L}^T \cdot (\mathbf{L} \cdot \mathbf{L}^T + \lambda \cdot \mathbf{I})^{-1} \cdot \Phi(t)$ , leading to the cortical source tomography as function of time.  $\lambda$  was the regularization parameter and selected via the generalized cross validation method [29] and  $\mathbf{I}$  was the identity matrix. The  $\lambda$  values at individual time points beyond three standard deviations of all time points from a participant were considered as outliers and interpolated with the neighboring ones.

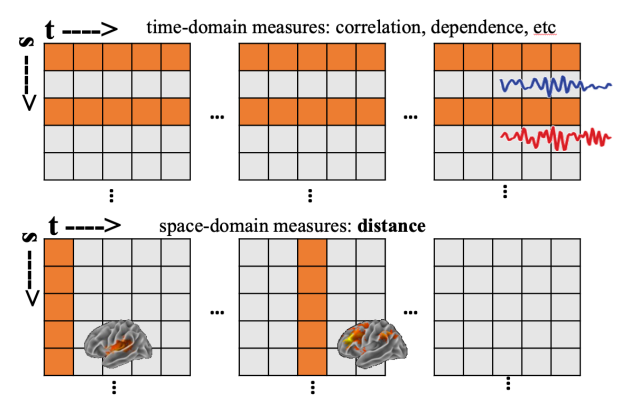


Fig. 1 1D time-domain and 3D spatial-domain measures for brain-wide activation patterns.

#### 2.3. Brain-wide CAPs and their Dynamics

To obtain bwCAPs, the following steps were performed on EEG cortical source tomography [30]. Firstly, cortical source tomographic data from each individual participant were filtered into data for the alpha band, i.e., 8-12Hz, and calculated for their instantaneous amplitudes [31, 32]. Secondly, cortical parcels were defined based on an atlas with each parcel representing cortical units of functional similarities [33]. To study the performance of the proposed approach at different spatial resolutions, two numbers (i.e., 100 and 200) of parcels were used. Thirdly, parcel-level instantaneous amplitude data were calculated as average values among all cortical sources within a parcel and converted into z scores at each individual participant. Lastly, cortical parcel-level z-score data were concatenated across participants and subject to a K-means clustering analysis using the L1-norm distance as the spatial-domain measure (Fig. 1) on the concatenated data to extract bwCAPs. The distance measure, different from time-domain measures, was calculated on single timeframe data (Fig. 1), which gave the highest possible temporal resolution that was only limited by the sampling rate. It was also noted that one-dimensional (1D) measures, e.g., correlation in time domain, were not appropriate to be used as the spatial-domain measures in the present study since the cortical surface spanned in the three-dimensional (3D) space and any calculation of 1D measures required vectorization of data from the higher-dimensional space into 1D that led to the loss of spatial relationship among individual cortical source points (Fig. 1). Meanwhile, the distance measure could reserve such spatial relationship in the high-dimensional space. For the protocol of running the K-means clustering, the cluster size was varied from 2 to 20, and the results from 12 clusters were reported based on the metric of explained variances [34].

The outcome of the K-mean clustering assigned individual timeframe data to a specific bwCAP, which led to a sequence of labels at the resolution of sampling frequency for identified bwCAPs. Thereafter, the spatial pattern of each bwCAP was obtained by averaging all time frames (z scores) belonging to the bwCAP. Two temporal metrics and one transitional metric were calculated for each bwCAP. An occurrence of a bwCAP was defined as multiple consecutive time frames that were assigned to the bwCAP, and counted in each participant. Lifetime was defined as the number of consecutive time frames in an occurrence of the bwCAP, and its mean value was firstly calculated in individual participants across all occurrences, and then averaged across all participants. These two temporal measures defined each bwCAP as a recurring transient brain state. One-step transition among states were defined as the transition from one CAP occurrence (at time t) to the next occurrence of a different CAP (at time t+1). The one-step transition rate was calculated via normalizing the number of one-step directional transitions (e.g., CAP1->CAP2 differs from CAP2->CAP1) toward the number of occurrences of the brain state at either time t+1 (i.e., inflow) or time t (i.e., outflow).

#### 3. RESULTS

For the spatial patterns from the cortical tomography of bwCAPs (Fig. 2 for 100 parcels), several distinct features are obtained. Firstly, large-scale distributed activations show in all bwCAPs (Fig. 5.1B and Fig. 4.2). Secondly, all bwCAPs indicate strong symmetry between two hemispheres. Lastly, these bwCAPs could also be visually conveniently grouped into three categories. The first category consists of bwCAPs 8, 9, 10 and 12 that have all their parcel-level z-scores across the whole cortex above the corresponding mean z-score levels (which is zero), indicating the global high-activation. Similarly, bwCAPs 2, 4, 5, and 7 indicate the global lowactivation as all their parcel-level z-scores lower than zero. At the same time, CAPs 1, 3, 6, and 11 indicate the non-global patterns with the parcel-level z-scores higher or lower than zero at different cortical locations. Moreover, an arrangement of bwCAPs in decreasing activation strengths, reflected similarly in both the global activation strength (i.e., sum of all parcels over the whole brain) and maximal parcel activation strength (numbers labeled in each bwCAP spatial map in Fig. 2), are observed within both the global highactivation and global low-activation groups. For example, in

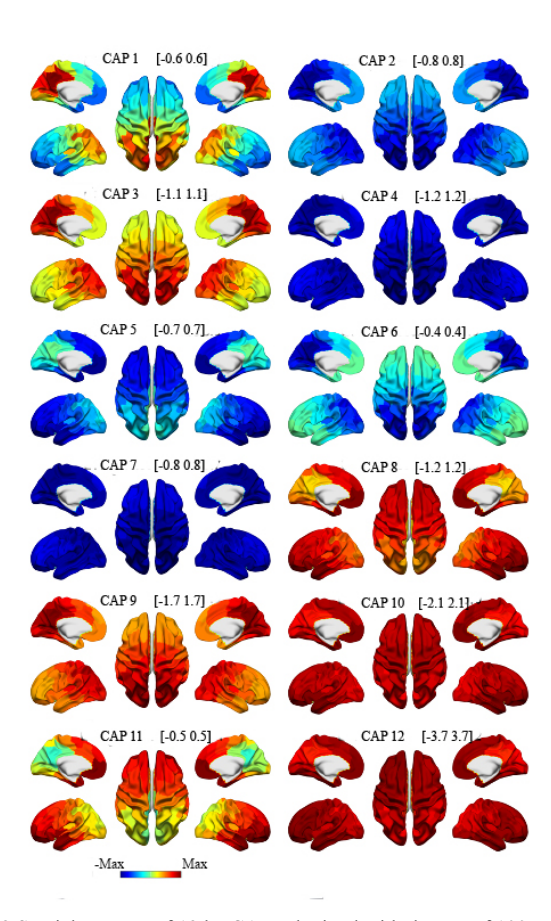


Fig. 2 Spatial patterns of 12 bwCAPs obtained with the use of 100 cortical parcels. Numbers in each subplot: maximal parcel activation amplitude.

the global high-activation group, the order of the bwCAPs in terms of activation amplitudes is 12, 10, 9, then 8. For the global low-activation group, the order is 4, 7, 2, then 5. It is also noted that the activation amplitude from the global highest-activation brain state (i.e., bwCAP 12) is more than 3 times of the activation amplitude from the global lowest-activation brain state (i.e., bwCAP 4). At the same time, the bwCAPs within the global low-activation group show much narrowed range of activation amplitudes among them, which might indicate that these bwCAPs are baseline brain states while the global high-activation bwCAPs indicate transient events that deviate from the baseline. The results using 200 parcels reveal the bwCAPs of similar spatial patterns as the bwCAPs from 100 parcels could be one-to-one matched to those from 200 parcels (Fig. 3).

The bwCAPs from these three groups further indicate distinct reproducible temporal and transitional characteristics (the top panel in Fig. 3). Typically, the global high-activation bwCAPs have relatively low occurrences (i.e., bwCAP 8, 9, 10, and 12). Most of the global low-activation bwCAPs have high occurrences (i.e., bwCAPs 4, 5, and 7). However, the global lowest-activation brain state (i.e., bwCAP 4) shows the similar low occurrences as the global high-activation bwCAPs. Furthermore, the global highest activation brain state (i.e., bwCAP 12) and the global lowest activation brain

state (i.e., bwCAP 4) display higher lifetimes than all other bwCAPs. Transitions between different brain states present moment-to-moment dynamics among these brain states in each recording session. Firstly, the one-step transition matrices (both inflow and outflow matrices) are sparse (Fig. 4), which supports the idea that transitions among these transient brain states are highly structured. Secondly, the onestep transitions occur more often between the bwCAPs from the same group, e.g., bwCAP 4 mostly transitioning to bwCAP 7 and both from the global low-activation group; bwCAP 12 mostly transitioning to bwCAP10 and both from the global high-activation group. This feature is similarly observed in both the inflow and outflow matrices (Fig. 4). All these distinct temporal and transitional features are reproduced in the results from 200 parcels (the low panel in Fig. 3).

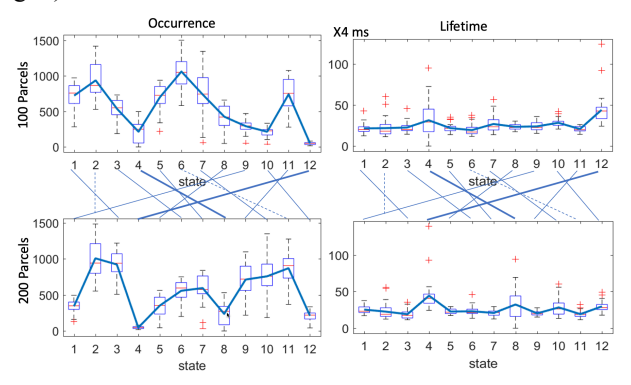


Fig. 3 Occurrences and lifetimes for 12 bwCAPs. Top panel: 100 cortical parcels; bottom panel: 200 cortical parcels; lines in the middle: one-to-one matched bwCAPs from 100 parcels and 200 parcels.

# 4. DISCUSSION

While fMRI has been dominant in studying brain-wide neuronal patterns in human brains, it is fundamentally limited in temporal resolutions due to the nature of hemodynamic responses [6]. EEG [7, 8] MEG [9] studies have been grown significantly in the past several years on researching brain-wide neuronal patterns because of their millisecond temporal resolutions. However, most of reported studies are still limited in temporal resolutions due to the similar choice of time-domain FC measures as fMRI. Our recent study has reported the detection of recurring transient brain states from broadband EEG data [22]. The present study adopted the use of a 3D spatial-domain measure, in place of 1D time-domain measures, which extended our previous detection of recurring transient brain states onto narrow-band resting rhythmic EEG oscillations (i.e., alpha band).

Interestingly, the set of bwCAPs reconstructed indicates layered activation strengths (i.e., the differences between the global high-activation and global low-activation groups, as well as ordered amplitudes for the bwCAPs with one of these groups), which might indicate that these brain-states are driven by low-occurrence transient events deviated from

baseline. The congruent evidence from spatial and temporal features of bwCAPs from the different groups further indicates the physiological significance of such recurring, while of low occurrence, transient events. For example, while the brain state with the strongest activation has the lowest occurrence, its lifetime is otherwise the highest. Then, the different roles played by the bwCAPs from the different groups further suggest that all spatial and temporal patterns might be driven by dynamic propagations of the recurring transient across the scale of whole brain.

In summary, we have detected the recurring transient brain-wide states modulating neuronal oscillations at resting human brains. This provides the first set of evidence that transient brain events occur in the frequency band that coherent neuronal oscillations are usually observed [21]. At the same time, such a phenomenon might be driven by propagating waves across the cortex [35] and responsible for correlation structures in spontaneous oscillatory activity [36].

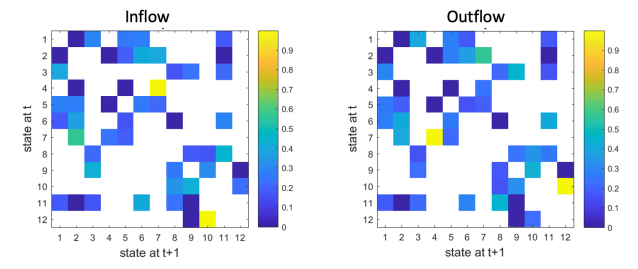


Fig. 4 Normalized one-step transitional probabilities. Left: inflow; right: outflow. White squares: zero transitional probabilities.

### 5. ACKNOWLEDGEMENT

The work was supported in part by NSF RII TRACK-2 FEC 1539068 and DARPA HR00112320032.

# 6. REFERENCES

- [1] M. D. Rosenberg *et al.*, "A neuromarker of sustained attention from whole-brain functional connectivity," *Nat Neurosci*, vol. 19, no. 1, pp. 165-71, Jan 2016, doi: 10.1038/nn.4179.
- [2] O. Sporns, "Network attributes for segregation and integration in the human brain," *Curr Opin Neurobiol*, vol. 23, no. 2, pp. 162-71, Apr 2013, doi: 10.1016/j.conb.2012.11.015.
- [3] B. Biswal, F. Z. Yetkin, V. M. Haughton, and J. S. Hyde, "Functional Connectivity in the Motor Cortex of Resting Human Brain Using Echo-Planar Mri," (in English), *Magnet Reson Med*, vol. 34, no. 4, pp. 537-541, Oct 1995, doi: DOI 10.1002/mrm.1910340409.
- [4] M. D. Fox and M. E. Raichle, "Spontaneous fluctuations in brain activity observed with functional magnetic resonance imaging," (in English), *Nat Rev Neurosci*, vol. 8, no. 9, pp. 700-711, Sep 2007, doi: 10.1038/nrn2201.
- [5] S. M. Smith *et al.*, "Correspondence of the brain's functional architecture during activation and rest," *Proc Natl Acad Sci U S A*, vol. 106, no. 31, pp. 13040-5, Aug 4 2009, doi: 10.1073/pnas.0905267106.
- [6] N. K. Logothetis, "What we can do and what we cannot do with

- fMRI," *Nature*, vol. 453, no. 7197, pp. 869-78, Jun 12 2008, doi: 10.1038/nature06976.
- [7] H. Yuan, L. Ding, M. Zhu, V. Zotev, R. Phillips, and J. Bodurka, "Reconstructing Large-Scale Brain Resting-State Networks from High-Resolution EEG: Spatial and Temporal Comparisons with fMRI," *Brain Connect*, vol. 6, no. 2, pp. 122-35, Mar 2016, doi: 10.1089/brain.2014.0336.
- [8] J. Britz, D. Van De Ville, and C. M. Michel, "BOLD correlates of EEG topography reveal rapid resting-state network dynamics," *Neuroimage*, vol. 52, no. 4, pp. 1162-70, Oct 1 2010, doi: 10.1016/j.neuroimage.2010.02.052.
- [9] M. J. Brookes *et al.*, "Investigating the electrophysiological basis of resting state networks using magnetoencephalography," *Proc Natl Acad Sci U S A*, vol. 108, no. 40, pp. 16783-8, Oct 4 2011, doi: 10.1073/pnas.1112685108.
- [10] B. Biswal, F. Z. Yetkin, V. M. Haughton, and J. S. Hyde, "Functional connectivity in the motor cortex of resting human brain using echo-planar MRI," *Magn Reson Med*, vol. 34, no. 4, pp. 537-41, Oct 1995, doi: 10.1002/mrm.1910340409.
- [11] J. L. Vincent *et al.*, "Intrinsic functional architecture in the anaesthetized monkey brain," (in English), *Nature*, vol. 447, no. 7140, pp. 83-U4, May 3 2007, doi: 10.1038/nature05758.
- [12] C. F. Beckmann, M. DeLuca, J. T. Devlin, and S. M. Smith, "Investigations into resting-state connectivity using independent component analysis," (in English), *Philos T Roy Soc B*, vol. 360, no. 1457, pp. 1001-1013, May 29 2005, doi: 10.1098/rstb.2005.1634.
- [13] J. Onton, M. Westerfield, J. Townsend, and S. Makeig, "Imaging human EEG dynamics using independent component analysis," (in English), *Neurosci. Biobehav. Rev.*, vol. 30, no. 6, pp. 808-822, 2006, doi: 10.1016/j.neubiorev.2006.06.007.
- [14] J. L. Chen, T. Ros, and J. H. Gruzelier, "Dynamic changes of ICA-derived EEG functional connectivity in the resting state," (in English), *Hum. Brain Mapp.*, vol. 34, no. 4, pp. 852-868, Apr 2013, doi: 10.1002/hbm.21475.
- [15] G. Shou and L. Ding, "Detection of EEG spatial-spectral-temporal signatures of errors: a comparative study of ICA-based and channel-based methods," (in English), *Brain Topo.*, vol. 28, no. 1, pp. 47-61, Jan 2015, doi: 10.1007/s10548-014-0397-z.
- [16] F. de Pasquale *et al.*, "Temporal dynamics of spontaneous MEG activity in brain networks," (in English), *P Natl Acad Sci USA*, vol. 107, no. 13, pp. 6040-6045, Mar 30 2010, doi: 10.1073/pnas.0913863107.
- [17] H. Luckhoo *et al.*, "Inferring task-related networks using independent component analysis in magnetoencephalography," (in English), *Neuroimage*, vol. 62, no. 1, pp. 530-541, Aug 1 2012, doi: 10.1016/j.neuroimage.2012.04.046.
- [18] C. Li *et al.*, "Cortical Statistical Correlation Tomography of EEG Resting State Networks," (in English), *Front Neurosci-Switz*, vol. 12, May 30 2018, doi: ARTN 365 10.3389/j.inins.2018.00365.
- [19] L. Ding, "Reconstructing cortical current density by exploring sparseness in the transform domain," *Physics in Medicine and Biology*, vol. 54, no. 9, pp. 2683-2697, 2009, doi: 10.1088/0031-9155/54/9/006.
- [20] K. Liao, M. Zhu, L. Ding, S. Valette, W. Zhang, and D. Dickens, "Sparse imaging of cortical electrical current densities via wavelet transforms," *Physics in Medicine and Biology*, vol. 57, no. 21, pp. 6881-6901, 2012, doi: 10.1088/0031-9155/57/21/6881.
- [21] P. Fries, "A mechanism for cognitive dynamics: neuronal communication through neuronal coherence," *Trends Cogn Sci*, vol. 9, no. 10, pp. 474-80, Oct 2005, doi: 10.1016/j.tics.2005.08.011.
- [22] L. Ding, G. Shou, Y. H. Cha, J. A. Sweeney, and H. Yuan,

- "Brain-wide neural co-activations in resting human," *Neuroimage*, vol. 260, p. 119461, Oct 15 2022, doi: 10.1016/j.neuroimage.2022.119461.
- [23] G. Shou, H. Yuan, Y. H. Cha, J. A. Sweeney, and L. Ding, "Age-related changes of whole-brain dynamics in spontaneous neuronal coactivations," *Sci Rep*, vol. 12, no. 1, p. 12140, Jul 15 2022, doi: 10.1038/s41598-022-16125-2.
- [24] A. Delorme and S. Makeig, "EEGLAB: an open source toolbox for analysis of single-trial EEG dynamics including independent component analysis," (in English), *J Neurosci Meth*, vol. 134, no. 1, pp. 9-21, Mar 15 2004, doi: 10.1016/j.jneumeth.2003.10.009.
- [25] H. Nolan, R. Whelan, and R. B. Reilly, "FASTER: Fully Automated Statistical Thresholding for EEG artifact Rejection," *Journal of Neuroscience Methods*, vol. 192, no. 1, pp. 152-162, 2010, doi: 10.1016/j.jneumeth.2010.07.015.
- [26] B. Fischl, "FreeSurfer," (in English), *Neuroimage*, vol. 62, no. 2, pp. 774-781, Aug 15 2012, doi: 10.1016/j.neuroimage.2012.01.021.
- [27] M. S. Hamalainen and J. Sarvas, "Realistic Conductivity Geometry Model of the Human Head for Interpretation of Neuromagnetic Data," (in English), *Ieee T Bio-Med Eng*, vol. 36, no. 2, pp. 165-171, Feb 1989, doi: Doi 10.1109/10.16463.
- [28] M. S. Hamalainen and R. J. Ilmoniemi, "Interpreting Magnetic-Fields of the Brain Minimum Norm Estimates," (in English), *Med Biol Eng Comput*, vol. 32, no. 1, pp. 35-42, Jan 1994, doi: Doi 10.1007/Bf02512476.
- [29] G. H. Golub, M. Heath, and G. Wahba, "Generalized Cross-Validation as a Method for Choosing a Good Ridge Parameter," (in English), *Technometrics*, vol. 21, no. 2, pp. 215-223, 1979, doi: 10.1080/00401706.1979.10489751.
- [30] L. Ding, G. Shou, Y. Cha, J. Sweeney, and H. Yuan, "Brainwide neural co-activations in resting human," *bioRxiv*, 2021.
- [31] J. F. Hipp, D. J. Hawellek, M. Corbetta, M. Siegel, and A. K. Engel, "Large-scale cortical correlation structure of spontaneous oscillatory activity," (in English), *Nat Neurosci*, vol. 15, no. 6, pp. 884-U110, Jun 2012, doi: 10.1038/nn.3101.
- [32] A. P. Baker *et al.*, "Fast transient networks in spontaneous human brain activity," *Elife*, vol. 3, p. e01867, Mar 25 2014, doi: 10.7554/eLife.01867.
- [33] A. Schaefer *et al.*, "Local-Global Parcellation of the Human Cerebral Cortex from Intrinsic Functional Connectivity MRI," (in English), *Cerebral Cortex*, vol. 28, no. 9, pp. 3095-3114, Sep 2018, doi: 10.1093/cercor/bhx179.
- [34] E. A. Allen, E. Damaraju, S. M. Plis, E. B. Erhardt, T. Eichele, and V. D. Calhoun, "Tracking Whole-Brain Connectivity Dynamics in the Resting State," (in English), *Cerebral Cortex*, vol. 24, no. 3, pp. 663-676, Mar 2014, doi: 10.1093/cercor/bhs352.
- [35] T. Matsui, T. Murakami, and K. Ohki, "Transient neuronal coactivations embedded in globally propagating waves underlie resting-state functional connectivity," *Proc Natl Acad Sci USA*, vol. 113, no. 23, pp. 6556-61, Jun 7 2016, doi: 10.1073/pnas.1521299113.
- [36] J. F. Hipp, D. J. Hawellek, M. Corbetta, M. Siegel, and A. K. Engel, "Large-scale cortical correlation structure of spontaneous oscillatory activity," *Nat Neurosci*, vol. 15, no. 6, pp. 884-90, Jun 2012, doi: 10.1038/nn.3101.